

**This is a self-archived version of an original article. This version may differ from the original in pagination and typographic details.**

**Author(s):** O'Donnell, David; Page, Robert D.; Grahn, Tuomas; Ali, Fuad; Auranen, Kalle; Capponi, Luigi; Carroll, Robert; Chishti, Muhammad Majid Rauf; Drummond, Mark; Greenlees, P. T.; Henderson, Jack; Herzan, Andrej; Jakobsson, Ulrika; Joss, David; Julin, Rauno; Juutinen, Sakari; Konki, Joonas; Labiche, Marc; Leino, Matti; Mason, Peter; McPeake, Christopher; Pakarinen, Janne; Papadakis, Philippos;

**Title:** High-spin states of 218Th

**Year:** 2020

**Version:** Published version

**Copyright:** © 2020 the Authors

**Rights:** CC BY 4.0

**Rights url:** <https://creativecommons.org/licenses/by/4.0/>

**Please cite the original version:**

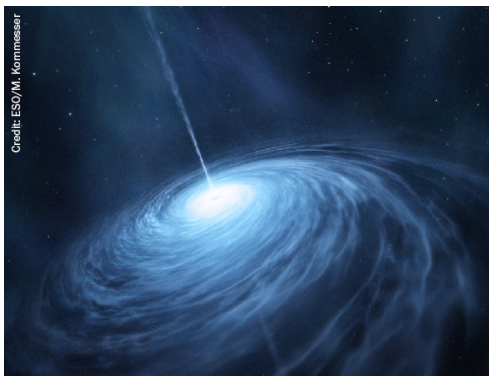
O'Donnell, D., Page, R. D., Grahn, T., Ali, F., Auranen, K., Capponi, L., Carroll, R., Chishti, M. M. R., Drummond, M., Greenlees, P. T., Henderson, J., Herzan, A., Jakobsson, U., Joss, D., Julin, R., Juutinen, S., Konki, J., Labiche, M., Leino, M., . . . Srivastava, P. C. (2020). High-spin states of 218Th. *Journal of Physics G: Nuclear and Particle Physics*, 47(9), Article 095103.  
<https://doi.org/10.1088/1361-6471/aba16c>

PAPER • OPEN ACCESS

## High-spin states of $^{218}\text{Th}$

To cite this article: D O'Donnell *et al* 2020 *J. Phys. G: Nucl. Part. Phys.* **47** 095103

View the [article online](#) for updates and enhancements.





AMERICAN  
ASTRONOMICAL  
SOCIETY

IOP | ebooks™

Your first choice for astronomy, astrophysics,  
solar physics, and planetary science ebooks.

Start exploring the collection—download the  
first chapter of every title for free.

# High-spin states of $^{218}\text{Th}$

D O'Donnell<sup>1,2,8</sup>, R D Page<sup>2</sup>, T Grahn<sup>3</sup>, F A Ali<sup>2,4</sup>,  
K Auranen<sup>3</sup>, L Capponi<sup>1</sup>, R J Carroll<sup>2</sup>, M M R Chishti<sup>1</sup>,  
M C Drummond<sup>2</sup> P T Greenlees<sup>3</sup>, J Henderson<sup>4,9</sup>,  
A Herzan<sup>3</sup>, U Jakobsson<sup>3</sup>, D T Joss<sup>2</sup>, R Julin<sup>3</sup>, S Juutinen<sup>3</sup>,  
J Konki<sup>3,10</sup>, M Labiche<sup>5</sup> M Leino<sup>3</sup>, P J R Mason<sup>5</sup>,  
C G McPeake<sup>2</sup>, J Pakarinen<sup>3</sup>, P Papadakis<sup>2</sup>, J Partanen<sup>3</sup>,  
P Peura<sup>3</sup>, P Rahkila<sup>3</sup>, J Revill<sup>2</sup>, P Ruotsalainen<sup>3</sup>,  
M Sandzelius<sup>3</sup>, J Sarén<sup>6</sup>, B Saygi<sup>2,11</sup>, C Scholey<sup>3</sup>,  
J Simpson<sup>5</sup>, J F Smith<sup>1</sup>, M Smolen<sup>1</sup>, J Sorri<sup>3,12</sup>,  
S Stolze<sup>3</sup>, C M Sullivan<sup>2</sup>, A Thornthwaite<sup>2</sup>, J Uusitalo<sup>3</sup>,  
A Kumar<sup>7</sup> and P C Srivastava<sup>7</sup>

<sup>1</sup> SUPA, School of Computing, Engineering and Physical Sciences, University of the West of Scotland, Paisley, PA1 2BE, United Kingdom

<sup>2</sup> Oliver Lodge Laboratory, University of Liverpool, Liverpool, L69 7ZE, United Kingdom

<sup>3</sup> University of Jyväskylä, Department of Physics, PO Box 35, FI-40014 University of Jyväskylä, Finland

<sup>4</sup> Department of Physics, College of Education, University of Sulaimani, P.O. Box 334, Sulaimani, Kurdistan Region, Iraq

<sup>5</sup> Department of Physics, University of York, Heslington, York YO10 5DD, United Kingdom

<sup>6</sup> STFC Daresbury Laboratory, Daresbury, Warrington, WA4 4AD, United Kingdom

<sup>7</sup> Department of Physics, University of Jyväskylä, PO Box 35, FI-40014, Jyväskylä, Finland

<sup>8</sup> Department of Physics, Indian Institute of Technology, Roorkee, Roorkee 247 667, India

E-mail: [david.odonnell@uws.ac.uk](mailto:david.odonnell@uws.ac.uk)

Received 9 April 2020, revised 15 June 2020

Accepted for publication 30 June 2020

Published 4 August 2020



CrossMark

<sup>9</sup> Author to whom any correspondence should be addressed.

<sup>10</sup> Lawrence Livermore National Laboratory, 7000 East Avenue, Livermore CA 94550 USA.

<sup>11</sup> Present address: CERN, CH-1211 Geneva 23, Switzerland.

<sup>12</sup> Present address: Department of Physics, Faculty of Science, Ege University, Bornova, Izmir, 35100, Turkey.; Department of Physics, Faculty of Science and Arts, Sakarya University, Sakarya 54187, Turkey.

<sup>13</sup> Present address: Sodankylä Geophysical Observatory, University of Oulu, Sodankylä, Finland.



Original content from this work may be used under the terms of the [Creative Commons Attribution 4.0 licence](https://creativecommons.org/licenses/by/4.0/). Any further distribution of this work must maintain attribution to the author(s) and the title of the work, journal citation and DOI.

**Abstract**

High-spin states in the  $N = 128$  nucleus  $^{218}\text{Th}$  have been investigated following fusion–evaporation reactions, using the recoil-decay tagging technique. Due to the short-lived nature of the ground state of  $^{218}\text{Th}$  prompt  $\gamma$  rays have been correlated with the  $\alpha$  decay of the daughter nucleus  $^{214}\text{Ra}$ . The level scheme representing the decay of excited states has been extended to  $(16^+)$  with the observation of six previously unreported transitions. The observations are compared with the results of shell model calculations and within the context of the systematics of neighbouring nuclei.

Keywords:  $\gamma$ -ray spectroscopy,  $\alpha$ -decay, shell model, thorium, fusion–evaporation reactions

(Some figures may appear in colour only in the online journal)

**1. Introduction**

Nuclei of the actinide region, particularly the isotopes of thorium with neutron number  $N \geq 126$ , have consistently been of interest throughout the last thirty years [1–5]. Possessing eight protons and  $(N - 126)$  neutrons outside of the well-studied doubly-magic  $^{208}_{82}\text{Pb}_{126}$ , these nuclei are an ideal laboratory in which to test the validity of shell-model interactions and to study the evolution of single-particle states away from closed shells.

Additionally, the Th isotopes with  $N \sim 126$  are in close proximity to a region of nuclei which have been shown to be influenced by strong octupole correlations [6]. These octupole correlations typically manifest themselves in low-lying negative parity states thought to result from octupole vibrations about a quadrupole-deformed core. Indeed, rotational bands built upon these low-lying states with strong interleaving E1 transitions are prevalent in the nuclei in this region and are regarded as a signature of this form of octupole collectivity [7]. The effect of these octupole correlations on the single-particle structure of the lighter ( $N \sim 126$ ) isotopes is also of interest from a shell model perspective.

A previous study of the nucleus  $^{218}\text{Th}$ , via conversion electron measurements, by Bonin *et al* [1] resulted in the observation of five excited states, with positive parity (up to spin  $10\hbar$ ). Measurements of the ratio of the observed number of  $K$ - and  $L$ -shell electrons established that the excited states are deexcited via stretched E2 transitions. No evidence for the low-lying negative-parity states that are observed in the heavier Th isotopes was reported. The fact that these states were not observed, in addition to the decreasing energy spacings between levels as a function of spin, has been interpreted as a sign of low collectivity [4].

One issue with the study of  $^{218}\text{Th}$ , and indeed the neighbouring Th isotopes, is the difficulty encountered in its production. The conventional method of producing these nuclei is via the evaporation of neutrons following fusion reactions. Although the evaporation of a neutron is considerably more likely than that of a charged particle, fission at each step of the fusion–evaporation process dominates.

The recoil-decay tagging (RDT) technique [8–10] was initially developed in order to study nuclei produced with low cross sections. This method, however, can also be useful in the study of nuclei produced in fusion–evaporation reactions in which fission is the dominant decay mechanism. Generally, this technique involves the coupling of two efficient detection systems at each end of a recoil separator. The spatial and temporal correlation of radiation detected in the low-background environment of the focal plane of the separator can then be correlated

with radiation detected at the target position. In the present work two arrays, one of germanium  $\gamma$ -ray detectors and the other of silicon detectors, were located at the target position while a pair of highly-segmented Si detectors were positioned at the focal plane of the separator.

The present work has resulted in the confirmation of the decay scheme reported by Bonin *et al* [1] and an extension of this level scheme with the observation of six previously unreported  $\gamma$ -ray transitions. The measured angular anisotropy of the  $\gamma$  rays indicates that four of the five excited states established here have negative parity, including a candidate  $J^\pi = 3^-$  state. The resulting level scheme is interpreted in terms of shell model excitations and the systematic behaviour of excited states in neighbouring nuclei.

## 2. Experimental details

The  $^{218}\text{Th}$  nuclei were produced via  $^{174}\text{Yb}(^{48}\text{Ca},4n)$  fusion–evaporation reactions. The target was  $0.85\text{ mg cm}^{-2}$  in thickness and had an isotopic enrichment of 98%. The beam of  $^{48}\text{Ca}^{10+}$  ions was accelerated to an energy of 207 MeV using the K130 cyclotron of the Accelerator Laboratory of the University of Jyväskylä for a total of 120 h.

LISA, an array of Si detectors, was located around the target position to detect charged particles emitted from the compound system or from short-lived states in the recoiling fusion–evaporation residues (recoils). The configuration of these detectors was based on that of the TIARA device [11] and consisted of Si strip detectors arranged in two coaxial octagonal barrels. The eight detectors comprising the inner barrel were  $300\text{ }\mu\text{m}$  thick and were each composed of four strips giving a total active area of  $22 \times 95\text{ mm}^2$ . The charge was read out from both ends of the strips thus providing longitudinal position sensitivity. The detectors of this inner barrel were located 33.8 mm from the beam axis and were shielded from scattered heavy ions by  $10\text{ }\mu\text{m}$ -thick Mo foils located 27.5 mm from the axis defined by the beam.

The eight detectors of the outer barrel were of  $500\text{ }\mu\text{m}$  thickness and provided a higher active area ( $28 \times 95\text{ mm}^2$ ) than the inner barrel detectors. These detectors were positioned 40.4 mm from the beam axis. An annular Si strip detector of  $300\text{ }\mu\text{m}$  thickness was also present 75.0 mm downstream of the target.

Around the Si detectors was the JUROGAM II array consisting of 34 high-purity escape-suppressed Ge detectors which facilitated the detection of prompt  $\gamma$  radiation. Ten of these detectors were of the EUROGAM Phase 1 [12] type and were located at  $133.6^\circ$  with respect to the beam direction. The other 24 detectors were of the Clover type [13] and were arranged in two groups with the detectors in each group at  $75.5^\circ$  and  $104.5^\circ$  with respect to the beam line. The target was located at the centre of the LISA barrels and the array of Ge detectors.

The recoils passed through the central hole of the annular Si detector of LISA and were subsequently separated from the unreacted beam using the RITU He-filled magnetic separator [14]. They were then transported to the RITU focal plane where they encountered the GREAT spectrometer [15]. The first component which the recoils encountered was a multi-wire proportional counter (MWPC) and were subsequently implanted into one of two double-sided Si strip detectors (DSSDs). The DSSDs were each of  $300\text{ }\mu\text{m}$  thickness and had an active area of  $60 \times 40\text{ mm}^2$ . Each strip had a pitch of 1 mm resulting in a total of 4800 pixels. In addition to the MWPC and the DSSDs, the GREAT spectrometer comprised a box of 28 Si PIN diode detectors, a planar Ge detector and four large-volume Ge detectors, one of which was of the clover type. The MWPC provided energy loss and (in conjunction with the DSSDs) time-of-flight information which was used to separate the recoils from any residual scattered beam. The signals from all detectors were passed to the total data readout acquisition system [16] where they were timestamped with a precision of 10 ns to facilitate temporal correlations

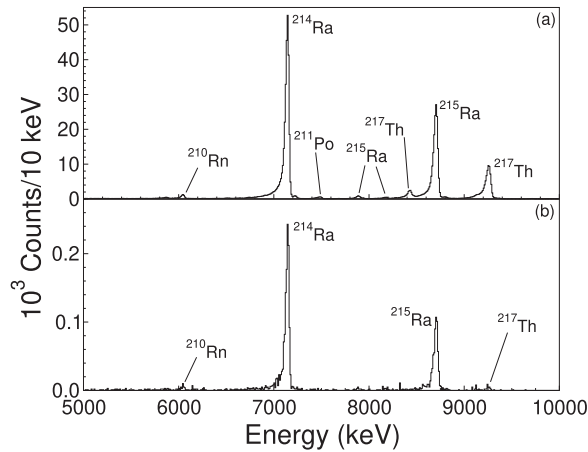


**Figure 1.** (a) All decays observed in the DSSDs within nine seconds of a recoil implantation in the same pixel. (b) Same as (a) but with the added condition that an event was observed in the annular detector of LISA. The origin of the labelled peaks is discussed within the text.

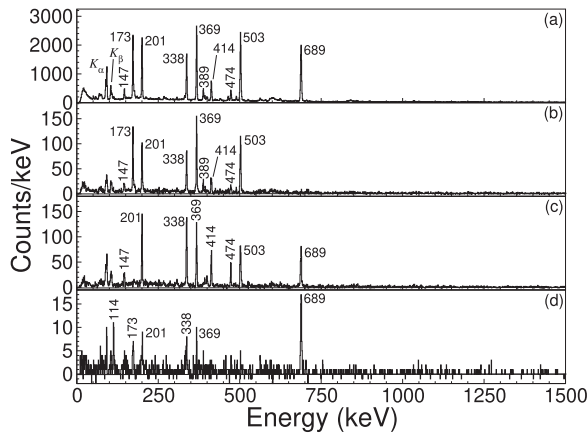


**Figure 2.** (a) Prompt  $\gamma$  rays correlated with the observation of the characteristic  $\alpha$  decay of  $^{214}\text{Ra}$ . Background-subtracted  $\gamma$ -ray spectra observed in coincidence with transitions of (b) 689 keV, (c) 173 keV and (d) 389 keV.

between the implantation of recoils in the DSSDs and both their prior and subsequent radioactive decays. The data were analysed using the Grain software package [17] and the Radware suite of programs [18].

### 3. Experimental results

In previous studies the ground state of  $^{218}\text{Th}$  has been reported to decay by emitting a 9666(10) keV  $\alpha$  particle [19]. The half-life of 117(9) ns [19] means that it is difficult to use this activity to perform conventional RDT. This is because, even with an ideal 100% transport

**Table 1.** Properties of  $\gamma$  rays associated with the decay of excited states of  $^{218}\text{Th}$  as a result of the present work. Intensities  $I_\gamma$  and  $I$  represent the measured  $\gamma$ -ray intensity and the transition intensity which has been corrected for internal conversion assuming no mixing of multipolarities. The intensities have been normalized with respect to the 689 keV  $2^+ \rightarrow 0^+$  transition. The angular anisotropy ratios,  $R$ , given in the table are discussed in the text. Spin and parity assignments are also listed.

$E_\gamma$ (keV)	$I_\gamma$	$I$	$R$	$J_i^\pi \rightarrow J_f^\pi$
114.2(7)	21(2)	29(3)	0.93(32)	$4^+ \rightarrow (3^-)$
146.7(5)	92(3)	110(4)	0.85(10)	$(16^+) \rightarrow (15^-)$
173.1(4)	443(8)	502(12)	0.93(3)	$(11^-) \rightarrow 10^+$
200.9(4)	416(7)	686(15)	1.23(5)	$8^+ \rightarrow 6^+$
337.8(5)	536(10)	600(14)	1.09(4)	$10^+ \rightarrow 8^+$
368.5(3)	767(13)	838(18)	1.21(4)	$6^+ \rightarrow 4^+$
388.9(6)	86(4)	88(4)	0.99(10)	$(3^-) \rightarrow 2^+$
413.7(4)	326(8)	348(10)	1.05(6)	$(13^-) \rightarrow (11^-)$
473.7(5)	206(6)	216(7)	1.08(9)	$(15^-) \rightarrow (13^-)$
503.3(3)	924(16)	963(22)	1.12(4)	$4^+ \rightarrow 2^+$
689.0(3)	1000(20)	1021(25)	1.13(4)	$2^+ \rightarrow 0^+$
$^{219}\text{Th}$ : 362	M1		0.90(12)	$11/2^+ \rightarrow 9/2^+$ [4]
$^{219}\text{Th}$ : 537	E2		1.10(7)	$13/2^+ \rightarrow 9/2^+$ [4]

efficiency of the recoil separator, only approximately 1% of all  $^{218}\text{Th}$  nuclei produced would survive the 0.5–1  $\mu\text{s}$  flight time from the target position to the focal plane. Instead it is the  $^{214}\text{Ra}$  nuclei, produced via the in-flight  $\alpha$  decay of  $^{218}\text{Th}$ , which are implanted and subsequently decay via  $\alpha$  emission.

The ground state of  $^{214}\text{Ra}$  has been reported to decay, predominantly (99.8%), via the emission of an  $\alpha$  particle of energy 7137 keV with a half-life of 2.46 s [20]. In the analysis of an RDT measurement the convention is to accept those radioactive decays which are observed in the same pixel into which the recoiling nucleus has been implanted and within some time interval. This correlation time is limited initially by the dead time of the electronics, which was approximately 13  $\mu\text{s}$ . The length of time over which the correlation of implantation and decay events can be correlated is limited only by the average implantation rate. In the case of the present work the average implantation rate was found to be approximately 50 Hz summed across both DSSDs. This means that the average time between successive implantations in a given pixel was approximately 67 s. The low implantation rate of the present work has meant that it has been possible to utilize long correlation times.

Figure 1(a) shows those  $\alpha$  decays which occur within nine seconds of the implantation of a recoil in the same pixel. The energy calibration of the DSSDs was performed using the known  $\alpha$  radiation of  $^{210}\text{Rn}$  (6041(3) keV [21]),  $^{215}\text{Ra}$  (8700(5) keV [22]) and  $^{217}\text{Th}$  (9261(4) keV [23]). The peak in figure 1 corresponding to the highest abundance of  $\alpha$  decays has an energy of 7142(5) keV which is in good agreement with the previously reported energy of the  $\alpha$  decay of the ground state of  $^{214}\text{Ra}$ .

In figure 2(a) is shown the prompt  $\gamma$  radiation observed at the target position associated with those recoils implanted into the DSSDs of the GREAT spectrometer and which have been followed, within 9 s, by the detection of an  $\alpha$  particle consistent with the known energy of the  $\alpha$ -decay of the ground state of  $^{214}\text{Ra}$ . Calculations using the code PACE, which is based on the work of reference [24], suggest that the cross section for the direct production of  $^{214}\text{Ra}$  nuclei is two orders of magnitude lower than that for the production of  $^{218}\text{Th}$ . This means that very few, if any, of the  $^{214}\text{Ra}$   $\alpha$  decays shown in figure 1(a) are the result of the direct population of

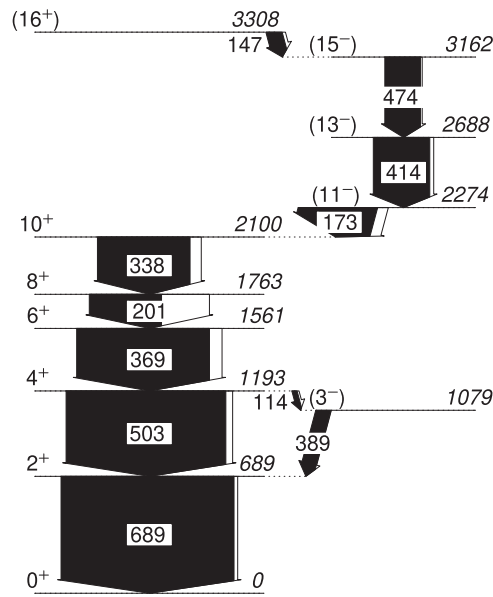


**Figure 3.** The level scheme representing the decay of excited states of  $^{218}\text{Th}$  established in the present work. The non-tentative spin and parity assignments reported in reference [1] have been included. Transition and level energies are given in units of keV and the widths of the arrows are proportional to the measured intensities of the transitions. The unfilled region of the arrows is indicative of internal conversion. The labels for the 114 keV and 147 keV transitions have been offset to show the arrows.

this nucleus. Instead it is proposed that these  $\alpha$  decays are the result of the in-flight  $\alpha$  decay of the  $^{218}\text{Th}$  nuclei. Support for this argument can be found in figure 2(a) in which there is no evidence of the 1382 keV  $2^+ \rightarrow 0^+$   $\gamma$ -ray transition [25] which would be observed if  $^{214}\text{Ra}$  was populated directly. In addition, the peaks in figure 2 identified as  $K_\alpha$  and  $K_\beta$  consists of three distinct peaks of energies of 90, 93 and 105 keV which are consistent with the known  $K_{\alpha 2}$ ,  $K_{\alpha 1}$  and  $K_{\beta 1}$  x-ray lines of Th.

Further support for the argument that the observed  $^{214}\text{Ra}$   $\alpha$  decays are not produced directly can be found in a comparison of figures 1(a) and (b) which are identical with the exception that the latter shows those  $\alpha$  decays correlated with events detected in the annular detector of LISA. Monte-Carlo simulations of the performance of the LISA detectors suggest that the detection efficiency of the annular detector is approximately 5% in the case of promptly-emitted charged particles of energies expected to result from this reaction. This efficiency is predicted to drop to 0.5% in the case of 9.7 MeV  $\alpha$  particles emitted with a half-life of 117 ns. The number of  $^{214}\text{Ra}$   $\alpha$  decays in figure 1(b) is 0.63(2)% of those in figure 1(a) which is close to the simulated efficiency. This result is consistent with the situation that the  $^{214}\text{Ra}$   $\alpha$  decays detected in the DSSDs of GREAT are not the result of the direct population of  $^{214}\text{Ra}$  nuclei following the fusion–evaporation reactions but are the result of the in-flight  $\alpha$ -decay of nuclei with properties consistent with those of the ground state of  $^{218}\text{Th}$ .

Eleven  $\gamma$ -ray transitions have been identified in the spectra of figure 2. The measured properties of these transitions are listed in table 1. Five of the observed transitions have been reported in an earlier study in which they were interpreted by Bonin *et al* [1] as a cascade of E2 transitions depopulating a  $J^\pi = 10^+$  state. The level scheme presented in the earlier work has been



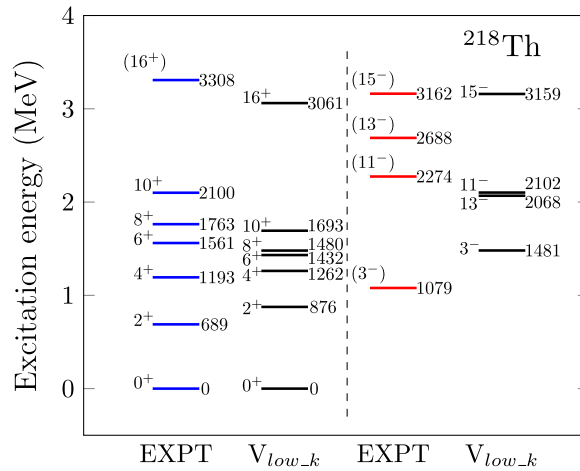


**Figure 4.** Comparison of experimental and theoretical energy levels for  $^{218}\text{Th}$ .

augmented with the addition of the six transitions identified as result of the present study. This level scheme is shown in figure 3. It should be noted that a 355 keV transition reported in reference [1] was not observed in the present study. The ordering of the  $\gamma$ -ray transitions has been established based on a  $\gamma\gamma$  coincidence analysis (examples of which can be seen in figures 2(b)–(d)) and their measured intensities. In determining the intensities, listed in table 1, the measured energy-dependent efficiency of the  $\gamma$ -ray detectors and the effects of internal conversion have been taken into account.

Conventional means of measuring the multipolarity of the  $\gamma$  radiation have proved difficult in the present work. Nonetheless, in an attempt to determine the spins and parities of the previously unreported excited states of  $^{218}\text{Th}$  the multipolarity of the  $\gamma$ -ray transitions has been investigated by exploiting the unique geometry of the Clover detectors which were located at angles close to 90 degrees with respect to the direction of the beam. In the case of the ring of twelve Clover detectors located at  $104.5^\circ$  they can be separated into two rings of twenty-four Ge crystals each located at angles of  $100^\circ$  and  $109^\circ$ . For each transition the efficiency-corrected intensity was measured in these rings and a ratio ( $R = I_\gamma(109^\circ)/I_\gamma(100^\circ)$ ) constructed. Informed by the well-known angular distribution of stretched dipole and quadrupole radiation from aligned nuclei, this ratio is expected to take on values less than unity for stretched dipole radiation and for stretched quadrupole transitions  $R > 1$ . The values of this ratio for each of the eleven transitions observed in the present work are given in table 1. Also listed in table 1 are ratios measured for a known magnetic dipole transition and an electric quadrupole transition in  $^{219}\text{Th}$ . The multipolarity of these transitions was previously established by Reviol *et al* [4].

#### 4. Large-scale shell model calculations

Large-scale shell model calculations were performed by taking  $^{208}\text{Pb}$  as a core with 82–126 model space for protons and 126–184 model space for neutrons. The valence proton model space included the six orbitals  $1f_{7/2}$ ,  $2p_{3/2}$ ,  $0h_{9/2}$ ,  $2p_{1/2}$ ,  $1f_{5/2}$ , and  $0i_{13/2}$  while the valence neutron model space comprised the seven orbitals  $1g_{9/2}$ ,  $0i_{11/2}$ ,  $0j_{15/2}$ ,  $2d_{5/2}$ ,  $3s_{1/2}$ ,  $1g_{7/2}$ , and  $2d_{3/2}$ . Calculations proceeded with an effective interaction derived from the CD-Bonn  $NN$

**Table 2.** The largest contributions to the configuration of wave functions for  $^{218}\text{Th}$ .

$J^\pi(\hbar)$	Wave function	Probability
$0^+$	$\pi(h_{9/2}^6 f_{7/2}^2) \otimes \nu(g_{9/2}^2)$	14%
$2^+$	$\pi(h_{9/2}^6 f_{7/2}^2) \otimes \nu(g_{9/2}^2)$	25%
$4^+$	$\pi(h_{9/2}^6 f_{7/2}^2) \otimes \nu(g_{9/2}^2)$	28%
$6^+$	$\pi(h_{9/2}^6 f_{7/2}^2) \otimes \nu(g_{9/2}^2)$	28%
$8^+$	$\pi(h_{9/2}^6 f_{7/2}^2) \otimes \nu(g_{9/2}^2)$	28%
$10^+$	$\pi(h_{9/2}^6 f_{7/2}^2) \otimes \nu(i_{11/2}^1 g_{9/2}^1)$	26%
$16^+$	$\pi(h_{9/2}^7 f_{7/2}^1) \otimes \nu(g_{9/2}^2)$	42%
$3^-$	$\pi(h_{9/2}^8) \otimes \nu(g_{9/2}^1 j_{15/2}^1)$	26%
$11^-$	$\pi(h_{9/2}^8) \otimes \nu(g_{9/2}^1 j_{15/2}^1)$	32%
$13^-$	$\pi(h_{9/2}^6 i_{13/2}^2) \otimes \nu(g_{9/2}^1 j_{15/2}^1)$	31%
$15^-$	$\pi(h_{9/2}^6 i_{13/2}^2) \otimes \nu(g_{9/2}^1 j_{15/2}^1)$	37%

**Table 3.** The shell model results for B(E2) values using effective charges  $e_p = 1.5 e$  and  $e_n = 0.5 e$ .

$J_i^\pi \rightarrow J_f^\pi$	B(E2) ( $e^2\text{fm}^4$ )
$2^+ \rightarrow 0^+$	462
$4^+ \rightarrow 2^+$	358
$6^+ \rightarrow 4^+$	258
$8^+ \rightarrow 6^+$	113
$10^+ \rightarrow 8^+$	11

potential using  $V_{\text{low}-k}$  renormalization approach [26]. For the calculation to be feasible, only two protons were permitted to be excited from  $0h_{9/2}$ ,  $1f_{7/2}$  to  $0i_{13/2}$  orbitals, while all neutron orbitals were open. The shell model code Antoine [27] was used to diagonalize the matrices, the dimensions of which involved in the present calculation for  $0^+$  state is  $\sim 90 \times 10^6$ . The results of calculated spectra are shown in figure 4. The largest configurations contributing to different levels are given in the table 2. We have also reported shell model results of B(E2) values for different transitions in the table 3. Effective charges corresponding to  $e_p = 1.5 e$  and  $e_n = 0.5 e$  have been used. The positive parity states up to  $J = 10\hbar$  are well connected with E2 transitions.

## 5. Discussion

The level scheme established by Bonin *et al* [1] has been confirmed in the present work and the angular anisotropies measured for the five previously reported  $\gamma$  decays are consistent with them being quadrupole transitions. In reference [1] it was reported that the  $J^\pi = 8^+$  and  $10^+$  states have half-lives of 1.2(2) and 0.3(2) ns. It has not been possible to confirm the lifetimes of these states using the apparatus employed in the present study.

A common feature of the even- $A$   $N = 128$  isotones is an isomeric  $J^\pi = 8^+$  state. Bonin *et al* [1] suggested that since the B(E2) of the  $8^+ \rightarrow 6^+$  decay continued to increase with increasing  $Z$ , that the dominant configuration of the  $8^+$  state has two neutrons occupying the lowest-energy valence orbital,  $g_{9/2}$ . The results of the present shell model calculations do indeed

support this assertion with this configuration accounting for  $\sim 28\%$  of the total wavefunction. In reference [1] it was argued that the main contribution to the wavefunction of the  $10^+$  state is the  $\nu(g_{9/2}^1 i_{11/2}^1)$  configuration. This too is supported by the shell model calculations reported here.

Four of the previously unreported transitions have been observed to be in coincidence with the five transitions first established by Bonin *et al* [1]. The most intense of these transitions, observed to feed the  $10^+$  state, has an energy of 173 keV. The angular anisotropy ratio for this decay is consistent with it being a stretched dipole transition suggesting that the 2274 keV state, from which it originated, most likely has  $J^\pi = 11^-$ . Further evidence for this transition being an electric dipole can be found by comparing the results of the present study with the results of reference [1]. In the present work the  $\gamma$ -ray intensities of the 173 and 201 keV transitions have been found to be very similar. Bonin *et al*, however, reported no evidence for conversion electrons associated with a transition of 173 keV suggesting that this transition does not have either M1 or E2 character. Furthermore, if the character of this transition was anything other than E1 then this would be the most intense transition in this nucleus.

There are few low-energy single-particle excitations in the relevant valence space which can result in a state of negative parity and spin  $11\hbar$ . One such configuration involves the excitation of a valence neutron to the  $j_{15/2}$  orbital. This is supported by the results of the shell model calculations which indicate that the largest contribution to the wavefunction of the negative parity states is the  $\nu(g_{9/2}^1 j_{15/2}^1)$  configuration.

The next most intense transitions have  $E_\gamma = 414$  and 474 keV. The measured angular anisotropies suggest that these transitions are stretched quadrupole in nature meaning that the most probable spins and parities of the decaying states are  $(13^-)$  and  $(15^-)$ , respectively. It is worth noting that the uncertainties associated with the angular anisotropy ratios means that the 414 and 474 keV transitions may also be dipoles. Excellent agreement is obtained between the observed energy of the proposed  $15^-$  state and the corresponding  $\pi(h_{9/2}^6 i_{13/2}^2) \otimes \nu(g_{9/2}^1 j_{15/2}^1)$ : 3159 keV shell model state.

A  $\gamma$ -ray transition of 147 keV was observed to feed the proposed  $(15^-)$  state. The measured properties of this decay indicate that this is most likely a dipole transition. It is unlikely that this transition is a magnetic dipole since, when internal conversion is taken into account, this would be one of the most intense transitions in the decay of excited states of  $^{218}\text{Th}$ . Instead it is more likely to be an electric dipole decay suggesting that the 3308 keV state from which it originates has  $J^\pi = (16^+)$ . This state is reproduced reasonably well by the shell model calculations indicating that the largest contribution to the wavefunction of this state is the  $\pi(h_{9/2}^7 f_{7/2}^1) \otimes \nu(g_{9/2}^2)$  configuration.

Two of the transitions first observed as a result of the present study have been observed in coincidence with all other  $^{218}\text{Th}$  decays with the exception of the 503 keV line ( $4^+ \rightarrow 2^+$ ) indicating that these by-pass this decay path. The angular anisotropy ratios measured for both of these transitions suggest that they are likely to be dipoles. If the 114 keV transition was of M1 character the Weisskopf estimate for the transition probability would be an order of magnitude larger than the estimated probability of the competing 503 keV E2 decay. This would mean that the 114 keV transition would dominate the decay of the  $4^+$  state. However, since the intensity of the 114 keV represents 3% of the decay of this state then it is more likely that this transition has E1 character. Therefore it is proposed that the state observed at 1079 keV has  $J^\pi = 3^-$ .

Support for the assignment of this spin and parity can be seen in figure 5 in which the excitation energies of  $3^-$  states in the Th isotopes have been plotted as a function of neutron number. The energy of the proposed  $3^-$  state in  $^{218}\text{Th}$  fits with the smooth parabolic trend already established in the Th isotopes, as highlighted in figure 5, which reaches a minimum for  $^{224}\text{Th}$  and  $^{226}\text{Th}$ . These thorium isotopes are those in which octupole correlations are thought

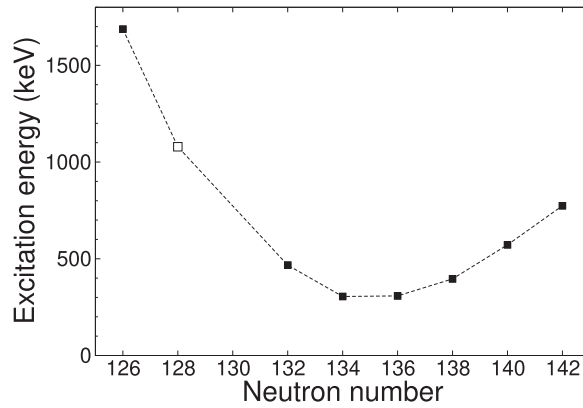


**Figure 5.** Excitation energies of  $J^\pi = 3^-$  states in thorium isotopes with  $N \geq 126$ . The unfilled data point corresponds to the result of the present work. The data, represented by the filled squares, have been extracted from references [2, 28–33].

to be strongest as evidenced by the observation of enhanced  $B(E1)/B(E2)$  ratios of  $10^{-6} \text{ fm}^{-2}$  [34, 35]. In the case of  $^{218}\text{Th}$  a measurement of the branching ratio of the decay of the  $4^+$  state provides a  $B(E1)/B(E2)$  ratio of  $4.96(49) \times 10^{-7} \text{ fm}^{-2}$ . Although Hauschild *et al* [2] reported no  $B(E1)/B(E2)$  ratio in their study of  $^{216}\text{Th}$ , the  $E1 4^+ \rightarrow 3^-$  transition appears to dominate the decay of the  $4^+$  state in that isotope. Inspection of the  $\gamma$ -ray spectra of reference [2] suggests a  $B(E1)/B(E2)$  ratio at least an order of magnitude higher than that measured here for  $^{218}\text{Th}$ .

Enhanced octupole correlations may result in a large electric dipole moment due to a shift in the centres of charge and mass of the nucleus. Dipole moments extracted from nuclei associated with such octupole correlations are exceptionally large corresponding to  $0.1\text{--}0.5 \text{ efm}$  [36]. An estimate of the intrinsic dipole moment,  $D_0$ , can be calculated based on  $B(E1)/B(E2)$  ratios and the intrinsic quadrupole moment,  $Q_0$ . The current experiment was not sensitive to the lifetimes of the excited states meaning that it has not been possible to measure the intrinsic quadrupole moment of the  $J^\pi = 4^+$  state. However, using the method prescribed by Grodzins [37], the intrinsic quadrupole moment can be estimated from the excitation energy of the first  $J^\pi = 2^+$  state. Using this value of  $Q_0 = 257 \text{ efm}^2$  the intrinsic dipole moment is calculated to be  $D_0 = 0.094(9) \text{ efm}$ . In the even–even thorium isotopes, the intrinsic dipole moment has values of  $0.11(2) \text{ efm}$  in  $^{228}\text{Th}$ , before reaching a maximum in  $^{224}\text{Th}$  ( $D_0 = 0.41(5) \text{ efm}$ ) and dropping again to  $0.25(3) \text{ efm}$  in  $^{220}\text{Th}$  [36]. The value determined here for  $^{218}\text{Th}$  fits well with this trend of decreasing  $D_0$  as the  $N = 126$  shell closure is approached.

In summary, the RDT technique has permitted the observation of  $\gamma$ -ray transitions associated with the decay of excited states in  $^{218}\text{Th}$ . The level scheme has been extended with the addition of five previously unreported states. Large-scale shell model calculations have been employed in order to gain an understanding of the microscopic structure of these excited states. A candidate  $J^\pi = 3^-$  state has been reported and, as a result, has permitted the measurement of a  $B(E1)/B(E2)$  ratio in this nucleus for the first time. The measured value of this ratio is consistent with the conclusions of previous studies of  $^{218}\text{Th}$  which suggested that this nucleus is near-spherical in shape and also indicates that  $^{218}\text{Th}$  exhibits a reduced degree of reflection asymmetry compared with that identified in the heavier isotopes.

## Acknowledgments

Financial support for this work has been provided by the UK Science and Technology Facilities Council (STFC) and by the EU 7th Framework Programme 'Integrating Activities—Transnational Access', Project No.: 262010 (ENSAR) and by the Academy of Finland under the Finnish Centre of Excellence Programme 2012-2017 (Nuclear and Accelerator Based Physics Programme at JYFL). TG acknowledges the support of the Academy of Finland, contract number 131665. The authors acknowledge the support of GAMMAPOOL for the loan of the JUROGAM detectors. The authors would also like to express their gratitude to the technical staff of the Accelerator Laboratory at the University of Jyväskylä for their support.

## ORCID iDs

D O'Donnell  <https://orcid.org/0000-0002-4710-3803>  
L Capponi  <https://orcid.org/0000-0002-2522-5463>  
M M R Chishti  <https://orcid.org/0000-0003-1246-7655>  
J Pakarinen  <https://orcid.org/0000-0001-8944-8757>  
B Saygi  <https://orcid.org/0000-0001-5406-506X>  
A Kumar  <https://orcid.org/0000-0003-3299-0435>

## References

- [1] Bonin W, Backe H, Dahlinger M, Glienke S, Habs D, Hanelt E, Kankeleit E and Schwartz B 1985 *Z. Phys. A* **322** 59
- [2] Hauschild K *et al* 2001 *Phys. Rev. Lett.* **87** 072501
- [3] Reviol W *et al* 2006 *Phys. Rev. C* **74** 044305
- [4] Reviol W *et al* 2009 *Phys. Rev. C* **80** 011304
- [5] Kuusiniemi P, Heßberger F P, Ackermann D, Hofmann S, Sulignano B, Kojouharov I and Mann R 2005 *Eur. Phys. J. A* **25** 397
- [6] Gaffney L P *et al* 2013 *Nature* **497** 199
- [7] Ahmad I and Butler P A 1993 *Annu. Rev. Nucl. Part. Sci.* **43** 71
- [8] Schmidt K-H *et al* 1986 *Phys. Lett. B* **168** 39
- [9] Simon R S, Schmidt K H, Heßberger F P, Hlavac S, Honusek M, Münzenberg G, Clerc H G, Gollerthan U and Schwab W 1986 *Z. Phys. A* **325** 197
- [10] Paul E S *et al* 1995 *Phys. Rev. C* **51** 78
- [11] Labiche M *et al* 2010 *Nucl. Instrum. Methods Phys. Res. A* **614** 439
- [12] Beausang C W and Simpson J 1996 *J. Phys. G* **22** 527
- [13] Duchêne G *et al* 1999 *Nucl. Instrum. Methods Phys. Res. A* **432** 90
- [14] Leino M 1997 *Nucl. Instrum. Methods Phys. Res. B* **126** 320
- [15] Page R D *et al* 2003 *Nucl. Instrum. Methods Phys. Res. B* **204** 634
- [16] Lazarus I H *et al* 2001 *IEEE Trans. Nucl. Sci.* **48** 567
- [17] Rahkila P 2008 *Nucl. Instrum. Methods Phys. Res. A* **595** 637
- [18] Radford D C 1995 *Nucl. Instrum. Methods Phys. Res. A* **361** 297
- [19] Wu S-C 2009 *Nucl. Data Sheets* **110** 681
- [20] Browne E 2003 *Nucl. Data Sheets* **99** 649
- [21] Kondev F G 2008 *Nucl. Data Sheets* **109** 1527
- [22] Singh B *et al* 2013 *Nucl. Data Sheets* **114** 661
- [23] Basunia M S 2007 *Nucl. Data Sheets* **108** 633
- [24] Gavron A 1980 *Phys. Rev. C* **21** 230
- [25] Stuchbery A E, Dracoulis G D, Kibédi T, Byrne A P, Fabricius B, Poletti A R, Lane G J and Baxter A M 1992 *Nucl. Phys. A* **548** 159
- [26] Coraggio L, Covello A, Gargano A and Itaco N 2009 *Phys. Rev. C* **80** 021305

- [27] Caurier E, Martínez-Pinedo G, Nowacki F, Poves A and Zuker A P 2005 *Rev. Mod. Phys.* **77** 427
- [28] Singh S 2011 *Nucl. Data Sheets* **112** 2851
- [29] Artna-Cohen A 1997 *Nucl. Data Sheets* **80** 227
- [30] Akovali Y 1996 *Nucl. Data Sheets* **77** 433
- [31] Artna-Cohen A 1997 *Nucl. Data Sheets* **80** 723
- [32] Browne E and Tuli J K 2012 *Nucl. Data Sheets* **113** 2113
- [33] Browne E 2006 *Nucl. Data Sheets* **107** 2579
- [34] Schwartz B, Ender C, Habs D, Schwalm D, Dahlinger M, Kankeleit E, Folger H, Simon R S and Backe H 1986 *Z. Phys. A* **323** 489
- [35] Ackermann B *et al* 1993 *Nucl. Phys. A* **559** 61
- [36] Butler P A and Nazarewicz W 1991 *Nucl. Phys. A* **533** 249
- [37] Grodzins L 1962 *Phys. Lett.* **2** 88